

# Geo-fit approach to the analysis of limb-scanning satellite measurements

Massimo Carlotti, Bianca Maria Dinelli, Piera Raspollini, and Marco Ridolfi

We propose a new approach to the analysis of limb-scanning measurements of the atmosphere that are continually recorded from an orbiting platform. The retrieval is based on the simultaneous analysis of observations taken along the whole orbit. This approach accounts for the horizontal variability of the atmosphere, hence avoiding the errors caused by the assumption of horizontal homogeneity along the line of sight of the observations. A computer program that implements the proposed approach has been designed; its performance is shown with a simulated retrieval analysis based on a satellite experiment planned to fly during 2001. This program has also been used for determining the size and the character of the errors that are associated with the assumption of horizontal homogeneity. A computational strategy that reduces the large number of computer resources apparently demanded by the proposed inversion algorithm is described. © 2001 Optical Society of America

*OCIS codes:* 010.1280, 010.1290, 010.4950, 280.0280, 280.1120.

## 1. Introduction

Limb-scanning measurements of the atmosphere are widely used to collect data on the vertical distribution of atmospheric constituents. In these measurements the spectrometer is carried at high altitudes by a flying platform and probes the Earth's limb at various depths in the atmosphere. Each observation is characterized by the altitude and the geolocation of the tangent point (that is, the point where the line of sight reaches the lowest altitude). A full set of measurements that covers the altitude interval of interest is usually referred to as a limb-scanning sequence.

Various methods have been proposed for the retrieval of physical and chemical atmospheric quantities from spectral features in limb-scanning measurements. Most of them make the assumption that the part of the atmosphere spanned by the lines of

sight of the limb-scanning sequence that is analyzed is horizontally homogeneous. In the case of a steady platform (typically a stratospheric balloon) the assumption of homogeneity applies to a length of several hundreds of kilometers. In the case of an orbiting platform the size of the atmospheric parcel sounded by a limb-scanning sequence increases because of the movement of the platform as the recording is made. If the direction of the line of sight is along the track of the orbit (along-track observations) the probed parcel could extend to a length approaching 2000 km (see, e.g., the test case described in Section 4 below). The atmospheric parameters that are retrieved with the assumption of horizontal homogeneity are expected to suffer an error induced by this assumption, especially in situations when strong variabilities, such as crossing of the terminator for photochemically active species and crossing of the antarctic polar vortex in ozone-hole conditions, are predicted.

From these considerations two problems arise: the first is how to evaluate the size and the character of the errors associated with the assumption of horizontal homogeneity and the second is how to avoid this assumption if the size of the induced errors is not acceptable.

Previous studies<sup>1,2</sup> have shown that the retrieval accuracy is particularly sensitive to horizontal temperature gradients; a temperature gradient of 3 K/100 km is reported to induce composition retrieval errors of tens of percent. A limited analysis

---

M. Carlotti (carlotti@safire.cineca.it) is with the Dipartimento di Chimica Fisica e Inorganica, Università di Bologna, Viale Risorgimento 4, 40136 Bologna, Italy. B. M. Dinelli is with the Istituto di Spettroscopia Molecolare del Consiglio Nazionale delle Ricerche, Via Gobetti 101, 40129 Bologna, Italy. P. Raspollini and M. Ridolfi are with the Istituto di Ricerca sulle Onde Elettromagnetiche del Consiglio Nazionale delle Ricerche, Via Panciatichi 64, 50127 Florence, Italy.

Received 7 June 2000; revised manuscript received 19 December 2000.

0003-6935/01/121872-14\$15.00/0

© 2001 Optical Society of America

of the effect on the retrieval errors of neglecting horizontal inhomogeneities is reported in Ref. 3. Bidimensional retrieval methods have been proposed<sup>4,5</sup> for the retrieval of temperature from nadir observations; they are based on tomography and analyze a parcel of the atmosphere measured with different observation geometries. A two-stage procedure that provides estimates of the horizontal gradients is described in Ref. 6 for a limb-sounding radiometer. More recently, a retrieval method has been presented<sup>7</sup> in which, in addition to the target quantity, the horizontal gradients are retrieved in the analysis of a limb-scanning sequence.

In this paper we propose a new approach to the retrieval of atmospheric parameters from limb-scanning observations that continually measure the atmosphere from an orbiting platform. It is based on the simultaneous analysis of observations taken along the whole orbit. In the case of along-track observations this approach fully accounts for the horizontal inhomogeneities encountered by the line of sight in the sounded atmosphere, so that these inhomogeneities are no longer a source of uncertainty for the retrieved quantities. Furthermore, this method makes full use of the information that originates from the geolocated positions sounded by the line of sight of each observation. A computing system that simulates satellite observations in the case of an inhomogeneous atmosphere and applies the proposed retrieval method has been designed. This system was used to analyze a few test cases that are based on the Michelson Interferometer for Passive Atmospheric Sounding (MIPAS), an experiment developed by the European Space Agency and planned to fly in 2001; this exercise has permitted the performance of the new approach to be assessed and also the errors caused by the assumption of horizontal homogeneity in a retrieval analysis to be characterized. Section 6 of this paper is dedicated to a description of the computational strategy that has been adopted to limit the demand for computer resources that seemingly would make dealing with the analysis problem impractical.

## 2. Rationale

In a limb measurement the signal that reaches the spectrometer is determined by the radiative-transfer processes along the whole line of sight. It follows that each observation contains information about all the locations that are spanned by the line of sight. However, inversion analyses that attempt to derive atmospheric parameters at different locations of the line of sight usually face an ill-posed problem that prevents retrieval of the desired information. The first-order approximation that is usually adopted is to consider that the information content of the observations comes entirely from the tangent point. This is the so-called onion-peeling method<sup>8</sup> in which the observed atmosphere is assumed to be horizontally homogeneous and one sequentially analyzes the limb observations to derive the unknown quantity at the altitude of the corresponding tangent point. In a second-order approximation the assumption of hori-

zontal homogeneity is maintained, but each limb observation is required to contribute to determining the unknown quantity at different altitudes among those spanned by its line of sight. This is the global-fit method<sup>9</sup> in which the retrieval problem can still be solved because all the observations of a limb-scanning sequence are merged in a simultaneous analysis. In a global fit the information about a given altitude is gathered from all the lines of sight that cross that altitude.

In a third-order approximation (which is the one of interest for the problem posed in Section 1) the assumption of horizontal homogeneity of the atmosphere is dropped. This means that each limb observation is required to contribute to determining the unknown quantity at a number of locations among those spanned by its line of sight. In this case the information about a given location cannot be gathered from observations of the same limb-scanning sequence (as in a global fit) because there are no common locations crossed by the lines of sight of a sequence.

In a satellite experiment one can solve the problem that arises when the assumption of horizontal homogeneity is dropped by exploiting the fact that limb-scanning measurements are continually repeated along the orbit. Figure 1 highlights the way in which the gathering of information can be achieved in the case of a satellite experiment that measures the atmosphere by looking backward along the track of the orbit. In this figure the lines of sight are represented (on a highly distorted scale) for a hypothetical limb-scanning sequence that is composed of four observation geometries; the tangent points of this sequence are marked with filled circles. Figure 1 also shows the tangent points of the sequences that immediately precede and follow the considered sequence; it can be seen that the lines of sight of the central sequence span a portion of the atmosphere that is also sounded by the observations of the nearby sequences. This means that the information about a given location of the atmosphere can be gathered from all the lines of sight that cross that location, whatever sequence they belong to. Inasmuch as the loop of cross talk between nearby sequences closes when the starting sequence is reached again at the end of the orbit, in a retrieval analysis one can gather complete information by merging the observations of a complete orbit into a simultaneous fit. We call this type of retrieval analysis a geo-fit.

## 3. Main Components of the Retrieval System

### A. Forward Model

The first and most important tool with which to implement the basic ideas that were described in Section 2 is a forward model that is capable of both simulating observations along a full orbit and accounting for the horizontal inhomogeneity of the atmosphere. This model, when it is calculating the signal that reaches the spectrometer, must be able to evaluate all the physical and chemical conditions that

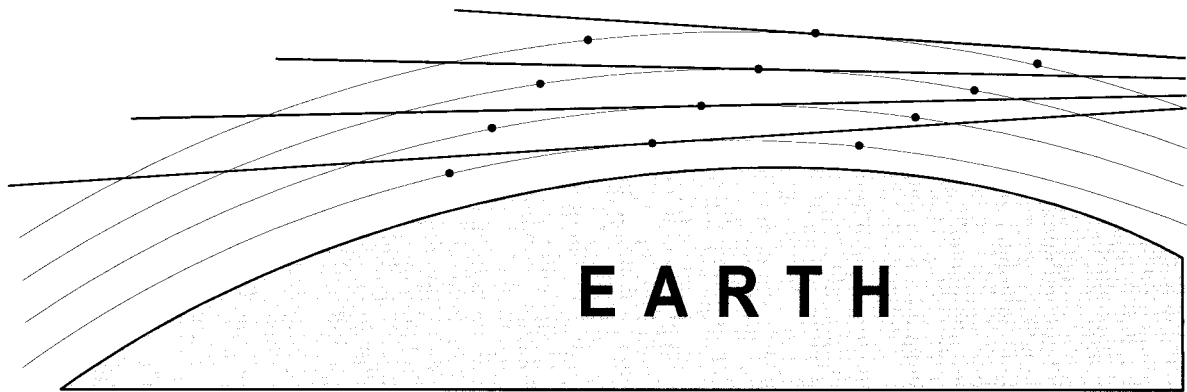


Fig. 1. Lines of sight for a satellite experiment that measures the atmosphere while looking backward along the track of the orbit. The tangent points of the limb-scanning sequence, plus those of two adjacent sequences, are marked by filled circles.

are encountered along the line of sight of a given observation. The overall sequence of operations and the mathematical optimizations of the forward model developed for this study are based on a model that was recently validated for simulations in horizontally homogeneous atmospheres; a thorough description of them can be found in Ref. 1. In this section we describe the main features that have been introduced into the forward model scheme to simulate the effects of the horizontal inhomogeneity of the atmosphere.

### 1. Assumptions

The main objective of this study was to develop a code for the study of the scientific aspects connected with the geo-fit approach. Therefore we have made the following assumptions: The atmospheric variability is considered only along the orbit's track, and it is assumed to be negligible in the cross-track direction. The Earth and the satellite orbit's shape are considered to be perfectly spherical. A planar polar-coordinate system is used to handle the geometric aspects of the problem, with the origin located at the Earth's center and the polar angle running on the plane that contains the orbit. The zero value of the polar angle is assumed to lie at the North Pole. Hereafter we shall refer to the polar-angle coordinate as an "orbital coordinate." In spite of the assumption of spherical symmetry, the gravity constant is considered to change with the geographic position. Because we are considering an experiment that continually measures the atmosphere, the forward model has been designed for emission measurements.

### 2. Atmospheric Model

The status of the atmosphere along the full orbit is represented by an input model that provides altitude profiles of pressure, temperature, volume mixing ratio (VMR) of the atmospheric species, and atmospheric continuum [provided as cross sections; see Eq. (2) in Subsection 3.A.7 below] at the frequencies that will be simulated. The profiles cover the altitude range of the observations up to a conventional value for the boundary of the atmosphere. A full set of altitude profiles is expected along the orbital coordinate

at grid points that cover the whole circumference of the orbit.

### 3. Discretization of the Atmosphere

The atmosphere is discretized on both coordinates of the reference system. On the radial coordinate, altitude levels are defined by use of criteria based on the altitude variations of both the temperature and the half-width of a reference transition.<sup>1</sup> These criteria are applied to the most unfavorable situation that can occur in the atmospheric model. The resultant layering is then extended to the whole orbit. On the orbital coordinate the atmosphere is discretized with regularly spaced radii that originate at the Earth's center. As a result, two geometric entities can be identified, and we shall call the point defined by the crossing of a level with a radius a node and the plane figure delimited by consecutive levels and radii a clove.

### 4. Definition of the Atmospheric Field

The values of physical and chemical quantities are calculated at the positions of all nodes starting from the input atmospheric model. Mixing ratios and temperatures are determined by linear interpolation with respect to both radial and orbital-coordinate values. Linear interpolation is also used for deriving the pressure at the nodes of the lowest altitude level; for the overhanging nodes the pressure is calculated from the hydrostatic-equilibrium equation applied along the radial coordinate. Finally, the atmospheric continuum is obtained by linear interpolation with respect to the orbital coordinate values and by linear interpolation with respect to the pressure values along the radial coordinate. It should be noted that the result of these two-dimensional operations can change when the order of the interpolating operations is reversed, with the differences approaching zero when the discretization of the atmosphere is reduced. For this reason the discretization of the atmosphere should be fine enough to provide a good approximation of the real situation (see Section 4 below).

## 5. Ray tracing

To perform ray tracing of each limb-scanning geometry we need to know the average coordinates of the spectrometer during the observation and the zenith angle that corresponds to the central line of sight of the instrument's field of view. These elements identify a straight line that reaches the boundary level of the atmosphere. Beginning at this point, the line of sight propagates into the atmosphere, crossing levels and radii following the discretization described in Subsection 3.A.3. At each intersection (with either levels or radii) the slope of the line of sight changes because of the variation of the refractive index, according to Snell's law. The resultant shape of a line of sight is therefore piecewise linear, with each segment representing the optical path ( $p$ ) within a clove. For each observation geometry two additional lines of sight are traced with zenith angles at the edges of the field-of-view pattern. The spectra that correspond to these three lines of sight are used to simulate the effect of the field of view by use of the convolution process described in Ref. 1.

## 6. Definition of Atmospheric Properties

Atmospheric properties are associated with each clove, starting from the quantities that have been calculated at the nodes that identify the clove itself. These properties are the average values of the refractive index and of the atmospheric continuum ( $c_{\text{cont}}$ ). Other atmospheric properties are associated with each individual path  $p$  (within a clove) that results from the ray tracing of a line of sight. These quantities, calculated for each spectroscopically active gas ( $g$ ) at the frequency of the simulation, are

- (1) slant column ( $\text{col}_{g,p}$ ),
- (2) equivalent pressures and temperatures, namely, the Curtis–Godson<sup>10</sup> quantities, and
- (3) absorption cross section ( $c_{g,p}$ ) calculated for the equivalent values of pressure and temperature.

## 7. Radiative Transfer

The radiative transfer is calculated for each line of sight with the classic formulas that refer to the case of no symmetry about the tangent point. For the reader's convenience we recall that one computes the signal  $S$  that reaches the spectrometer by approximating the radiative-transfer integral as a summation over the  $N$  paths that compose the line of sight:

$$S = \sum_{p=1}^N B_p [1 - \exp(-\tau_p)] \left[ \prod_{k=p+1}^N \exp(-\tau_{k,p}) \right], \quad (1)$$

where  $\tau_p$  is the single-path optical depth, given by

$$\tau_p = \sum_{g=1}^{N_{\text{gas}}} c_{g,p} \text{col}_{g,p} + c_{\text{cont},p} \text{col}_{\text{air},p} \quad (2)$$

and  $B_p$  is the Planck function computed for the equivalent temperature of the target gas of the retrieval. In the second term of Eq. (2)  $c_{\text{cont},p}$  represents the contribution to the single-path optical depth of all the

emission sources characterized by a constant amplitude in a limited spectral interval (the contribution of atmospheric continuum);  $\text{col}_{\text{air},p}$  is the air column for path  $p$ .

## B. Retrieval Procedure

The retrieval system derives VMR values of a given molecular species from the observations of a whole orbit. The parameters of the retrieval are

- (1) VMR values of the analyzed molecular species at a set of geolocated altitudes (retrieval grid) and
- (2) atmospheric continuum values, at the same position of VMR parameters, for the frequency of the analyzed observations.

### 1. High-Level Mathematics

The parameters of the retrieval are derived from a nonlinear least-squares fit based on the Gauss–Newton method. The high-level mathematics of this method, applied to the retrieval of atmospheric parameters, can be found in Refs. 1 and 11. Here we note some concepts that will be used in the following sections of this paper.

The Gauss-Newton iterative solution formula is

$$\mathbf{y} = (\mathbf{K}^T \mathbf{S}_n^{-1} \mathbf{K})^{-1} \mathbf{K}^T \mathbf{S}_n^{-1} \mathbf{n}, \quad (3)$$

where  $\mathbf{y}$  is a vector that contains the corrections to the assumed value of the parameters,  $\mathbf{n}$  is a vector that contains the difference between each observation and the corresponding simulation,  $\mathbf{S}_n$  is the variance–covariance matrix associated with the vector  $\mathbf{n}$ , and  $\mathbf{K}$  is the matrix (usually denoted a Jacobian matrix) that contains the derivatives of the observations with respect to each parameter.

In the case of a Gaussian distribution of the measurement errors, Eq. (3) provides the solution that minimizes the  $\chi^2$  function, defined as

$$\chi^2 = \mathbf{n}^T \mathbf{S}_n^{-1} \mathbf{n}. \quad (4)$$

The quantity  $q$ , defined as

$$q = \frac{\chi^2}{(m - n)}, \quad (5)$$

where  $m$  is the number of observations and  $n$  is the number of retrieved parameters, has an expectation value of 1. Therefore the deviation of  $q$  from unity provides a good estimate of the quality of the retrieval.

The errors associated with the solution of the inversion procedure can be characterized by the variance–covariance matrix of  $\mathbf{y}$ , given by

$$\mathbf{V}_y = (\mathbf{K}^T \mathbf{S}_n^{-1} \mathbf{K})^{-1}. \quad (6)$$

Matrix  $\mathbf{V}_y$  maps the experimental random errors (represented by  $\mathbf{S}_n$ ) onto the uncertainty of the values of the retrieved parameters; in particular, the square root of the diagonal elements of  $\mathbf{V}_y$  provides the estimated standard deviation (ESD) of the corresponding parameter.

The following part of this subsection focuses on the features that were introduced in the retrieval scheme to handle the problems associated with retrievals that model the horizontal inhomogeneity of the atmosphere.

## 2. Retrieval Grid

The spatial resolution and the accuracy with which the retrieved profile is determined are generally anticorrelated<sup>11</sup> and are strongly dependent on the grid on which the retrieved points are represented. When horizontal homogeneity is assumed in the atmosphere the problem of choosing the retrieval grid lies in the selection of the altitudes where the parameters will be retrieved. Inasmuch as the weighting functions<sup>11</sup> of the observations generally peak at the tangent altitudes, a common choice is to have these altitudes coincide with the retrieval grid. In the case of a geo-fit, a two-dimensional retrieval grid must be adopted, where the orbital coordinate is the second dimension. The locations of the tangent points of the observations (see Fig. 1) along the whole orbit could still be the leading criterion for the choice of the retrieval grid. However, even in the case of identical elevation scans, because of the inhomogeneity of the atmosphere, the ray tracing of the observations leads to different tangent altitudes because of the different refractive indices encountered by the lines of sight. The resultant spread of the tangent altitudes would make the interpolation process complex, so a retrieval grid at fixed altitudes is a more suitable choice. The choice can be driven by the nominal position of tangent points, that is, the position of the tangent point in the absence of refraction along the lines of sight. In the retrieval system discussed in this paper the retrieval grid can be either automatically set by the code at the nominal location of tangent points or defined through an input file.

## 4. Performance of the Retrieval Method

To assess the performance of the proposed retrieval concept it would be desirable to apply the idea to real measurements. In the absence of real observations we tested the system on a few cases based on the MIPAS instrument, which is expected to fly in 2001 onboard Environmental Satellite-1 (ENVISAT-1), a satellite of the European Space Agency. A detailed description of this experiment can be found in Ref. 12. Here we briefly describe the main features of the experiment that are relevant for the retrieval analyses.

### A. MIPAS Experiment

The MIPAS will measure the atmospheric-limb emission over a spectral interval ranging from 685 to 2410  $\text{cm}^{-1}$  with a spectral resolution of 0.035  $\text{cm}^{-1}$  (unapodized). In this region the spectrum contains features of most atmospheric constituents. Therefore one can process MIPAS limb-scanning observations to determine the altitude distribution of many physical and chemical quantities. The retrieval of pressure and temperature as well as of the VMR of five

high-priority species, namely,  $\text{O}_3$ ,  $\text{H}_2\text{O}$ ,  $\text{HNO}_3$ ,  $\text{CH}_4$ , and  $\text{N}_2\text{O}$ , will be routinely performed by the European Space Agency in nearly real time.

The redundancy of information coming from the broadband MIPAS spectra makes it possible to select a set of narrow (less than 3  $\text{cm}^{-1}$ ) spectral intervals, called microwindows, that contain the best information on the target quantities. A database containing the definition of the microwindows and all the quantities that are needed to simulate the atmospheric spectrum will be associated with each target species.

Several observation modes that are focused on various regions of the atmosphere are foreseen. Our test cases have been based on the standard observation mode, which will be routinely used for most of the observation time. For operation in this mode, the MIPAS measures limb-scanning sequences by looking backward along the orbit track. The elevation scan ranges from 53 to 8 km in 3-km steps. The recording time for a spectrum is 4.5 s; the time for a complete elevation scan is  $\sim 75$  s. As the ENVISAT-1 orbiting period is  $\sim 100$  min, the MIPAS will repeat 80 limb-scanning sequences along a full orbit in the standard observation mode.

The ray tracing for the MIPAS standard observation mode (that is, Fig. 1 drawn to the appropriate scale) shows that the lines of sight for each limb-scanning sequence span a region of the atmosphere that extends for  $\sim 2000$  km. This region is sounded by the observations of three nearby sequences. The separation between two contiguous MIPAS sequences corresponds to  $\sim 4.5^\circ$  in the orbital coordinate.

### B. Atmospheric Model

We needed to select a realistic atmospheric model with which to test the new system. We adopted the SLIMCAT three-dimensional chemical transport model developed by Chipperfield.<sup>13</sup> This model provides pressure, temperature, and VMR altitude profiles on a grid  $7.5^\circ$  in longitude and  $5^\circ$  in latitude, except for the polar regions where the latitudinal grid is  $4.5^\circ$ . The status of the atmosphere was calculated for one day, 27 September 1996. The atmospheric model was integrated with atmospheric-continuum profiles. These profiles are calculated by use of the model described in Ref. 14. The test case reported in this paper refers to the atmosphere encountered by the polar orbit that overpasses Greenwich (for the sake of simplicity we considered a strictly polar orbit, whereas a slight inclination is foreseen for the ENVISAT-1 orbit).

### C. Validation of the Forward Model

A validation of the forward model would require a comparison of spectra simulated by our code with spectra simulated by a reference code that is already validated. A successful comparison performed in this way would represent a sufficient condition for the validation. Because no reference code is available for the calculation of spectra that will take into account horizontally inhomogeneous atmospheres, we

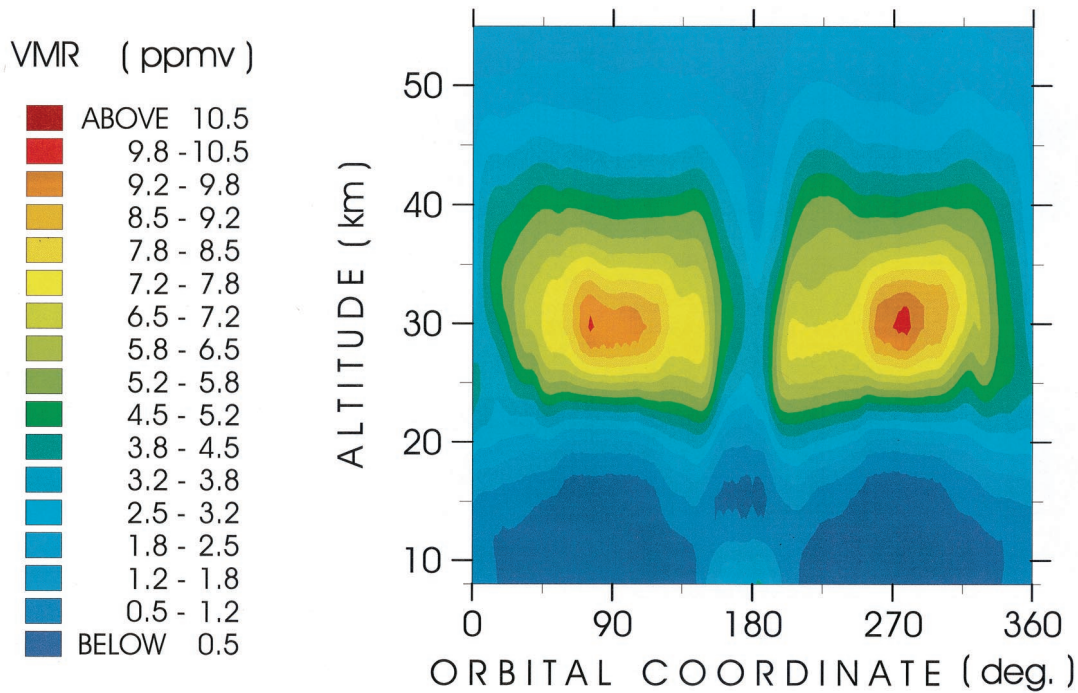


Fig. 2. Ozone distribution along the orbit selected for the retrieval test. VMR values are represented by different colors as a function of altitude and orbital coordinate. (ppmv, Parts in  $10^6$  by volume.)

adopted two criteria that, represent necessary conditions for the validation. They are that, when the forward-model code works on a horizontally homogeneous atmosphere, the code must provide identical spectra for identical observation geometries of different limb-scanning sequences along the whole orbit and must provide spectra that are identical to those calculated by a reference code already validated for horizontally homogeneous atmospheres.

To be able to check whether these criteria are fulfilled, we built a horizontally homogeneous atmospheric model. Observations relative to a full orbit were simulated for this atmosphere over a few tens of frequency intervals that correspond to MIPAS microwindows. Then spectra that correspond to identical observation geometries of different limb-scanning sequences were compared. The comparison showed that differences exist and have an amplitude that exhibits a quasi-periodic behavior when consecutive limb-scanning sequences are compared to a reference sequence. These differences are explained by the size of the atmospheric subdivision (see Subsection 3.A.3). In fact, the maximum amplitude of the observed differences decreases, and can be reduced below a given threshold, with refinement of the atmospheric discretization.

We found the same behavior when we compared spectra of consecutive limb-scanning sequences with those of a reference sequence that is generated by the optimized forward model<sup>1</sup> (already validated for horizontally homogeneous atmospheres). In this case one can reduce the maximum difference between the compared spectra below a given threshold by refining

the atmospheric discretization in both forward models.

#### D. Performance of the Retrieval System

We tested the retrieval system by carrying out geo-fit analyses on simulated MIPAS observations (generated by the forward model described in Subsection 3.A). The initial-guess profiles of the retrievals were perturbed with respect to the reference profiles (those employed to generate the simulated observations). The retrieved VMR values and their ESD's were then evaluated with respect to the values provided by the reference profiles.

In this subsection we describe the procedure that we followed to simulate a geo-fit retrieval of ozone VMR. The atmospheric model (see Subsection 4.B) refers to ozone-hole conditions in the Antarctic; therefore strong horizontal gradients were expected in the atmosphere. Figure 2 shows the ozone distribution along the selected orbit. In this figure the VMR values are represented by different colors as a function of altitude and orbital coordinate (the South Pole is at  $180^\circ$ ). The latitudinal resolution of the atmospheric model (see Subsection 4.B) is fine enough to generate situations in which ozone gradients change sign along the lines of sight of MIPAS observations. Therefore the retrieval system should handle oscillations of the VMR value and not simply constant gradients.

MIPAS observations were simulated over a set of microwindows selected from a preliminary database prepared for ozone.<sup>15</sup> Gaussian random noise (provided by the MIPAS radiometric specifications) was

Table 1. Performance of Geo-Fit for Ozone VMR Retrieval

Altitude (km)	Average ESD (%)	Maximum ESD (%)	Orbital Coordinate	Average Deviation (%)	Maximum Deviation (%)	Orbital Coordinate
53	4.0	6.1	352.0	2.4	8.0	104.7
50	5.7	8.7	352.0	3.8	12.6	37.2
47	4.4	8.0	347.9	2.8	10.8	347.9
44	3.1	5.6	357.2	1.9	8.0	222.2
41	2.4	4.9	352.0	1.6	6.3	294.4
38	2.1	4.3	352.0	1.4	4.6	347.9
35	2.0	4.2	357.2	1.4	5.0	321.8
32	2.1	3.8	347.9	1.6	6.5	357.2
29	2.5	3.9	11.8	2.0	6.1	340.9
26	3.5	4.9	241.5	2.6	9.0	241.5
23	3.2	5.1	174.2	1.9	7.2	169.7
20	3.1	9.0	165.5	1.8	6.0	174.2
17	4.8	16.5	269.2	2.7	16.8	269.2
14	6.0	17.9	269.2	4.6	22.6	179.4
11	2.9	6.4	89.6	2.1	7.3	103.1

added to the simulated spectra. The discretization of the atmosphere that was adopted (see Section 4) was such that, for a homogeneous atmosphere, the maximum amplitude of the differences between identical geometries (see Section 4.C) was less than a factor of 0.25 with respect to the smallest value of noise-equivalent spectral radiance, that is,  $2 \text{ nW}/(\text{cm}^2 \text{ sr cm}^{-1})$ . In this discretization the separation between radii is of the order of 100 km at ground level (that is, approximately one fifth of the distance covered by tangent points within a limb-scanning sequence). We obtained the initial-guess profiles for the retrievals by applying a perturbation factor to the reference profiles; this factor was different for each profile and was determined by a random-numbers generator within given thresholds. The applied threshold was  $\pm 30\%$  for ozone VMR and  $\pm 50\%$  for the atmospheric continuum. The retrieval grid was defined by the nominal location of the tangent altitudes.

In this test case, the geo-fit required just one Gauss-Newton iteration to reach convergence. Table 1 provides an overall picture of the quality of this retrieval. Column 1 of this table lists the altitudes of the retrieval grid; column 2, the average percent value of the ESD calculated over the 80 grid points at that altitude in the retrieval grid. The maximum values of the ESD at that altitude are listed in column 3, and the orbital coordinates where the maximum values occur are listed in column 4. Columns 5, 6, and 7 contain entries that are analogous to those of columns 2, 3, and 4, respectively. These entries refer to the absolute deviations of the retrieved VMR's with respect to the reference values (that is, the value at that grid point derived from the reference profiles). The ESD's reported in this paper are scaled by the quantity  $q$  defined in Eq. (5) (see Section 5 below for an explanation of reason for this choice). However, at convergence,  $q$  was 1.02, so the values listed in Table 1 coincide, in practice, with the random errors that are due to spectral noise. Table 1 shows that, on average, the reference VMR values have been recovered quite well; furthermore, the de-

viations with respect to the reference values lie within the ESD calculated by the retrieval system. We have listed in Table 1 the maximum values of both percent ESD and percent deviation to show how they can degrade the average values. The maximum errors generally occur at geographic locations where the amount of ozone is nearly zero; the extreme case occurs at 8 km, where, in some locations, percent errors are so big as to force the average values above 100%. These meaningless values are not included in the table. Table 1 also shows that maximum errors tend to occur near the North Pole, where the orbit was started. This is so because all the sequences are equally spaced (in terms of the orbital coordinate) except for the last and the first ones, each of which is closer to its neighbor because of the imposed constraint of fitting an integer number of sequences within the orbit. What we observe from Table 1 is therefore a consequence of the trade-off between the horizontal resolution and the accuracy of the retrieved parameters. This consideration suggests that, in the case of a geo-fit, the trade-off between accuracy and spatial separation of the observations has to be assessed. The spatial resolution is, in turn, related to the spectral resolution of the instrument through the recording time of each observation geometry.

Figures 3 and 4 show the results of the retrieval test in a form obtained by use of software that generates maps by interpolating discrete values. These figures represent, respectively, percent ESD's and absolute deviations of the retrieved VMR values over the whole orbit; the agreement between these quantities can be appreciated from these figures. Furthermore, a comparison of Figs. 3 and 4 with Fig. 2 shows that the errors are not correlated with horizontal variability along the orbit.

### 5. Errors Originated by the Assumption of Horizontal Homogeneity

In this section we evaluate the size and the character of the errors associated with the assumption of hor-

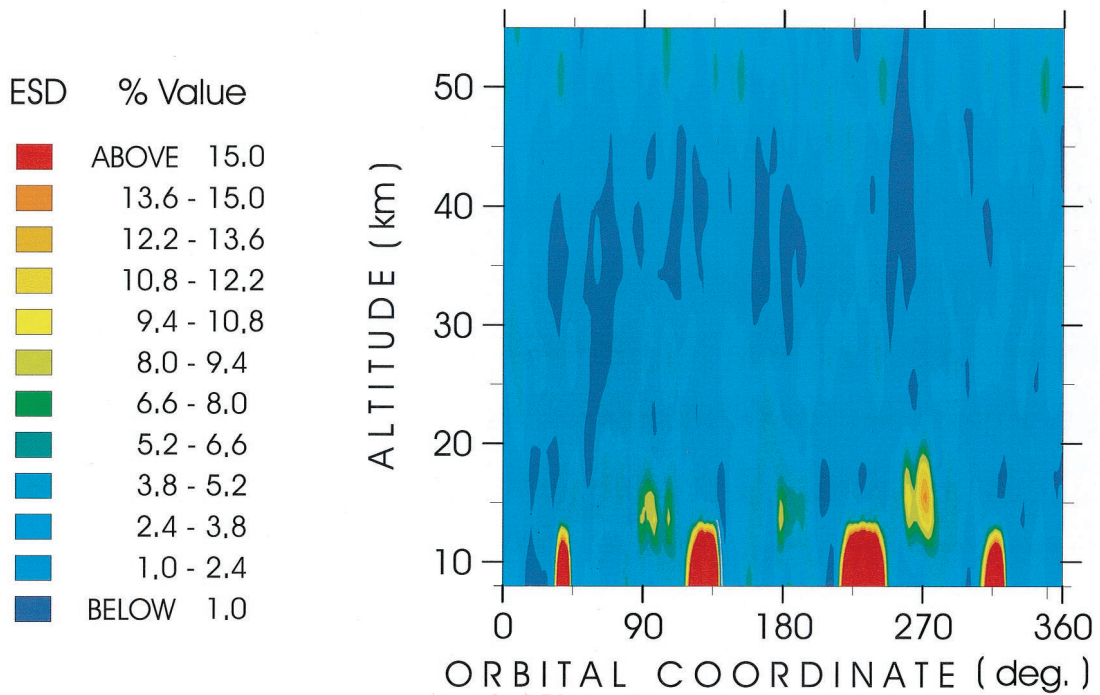


Fig. 3. Values of the ESD obtained by the geo-fit as a function of altitude and orbital coordinate.

horizontal homogeneity in a retrieval analysis. For this purpose we performed retrievals using a code that makes the horizontal homogeneity assumption on observations simulated with a horizontally inhomogeneous atmosphere was assumed. A comparison of the errors that result from these retrievals with those

that result from the geo-fit will provide the desired information.

For the analyses with the assumption of horizontal homogeneity we used the optimized retrieval model<sup>1</sup> (ORM) that was specifically designed for MIPAS observations. We show the comparison between the

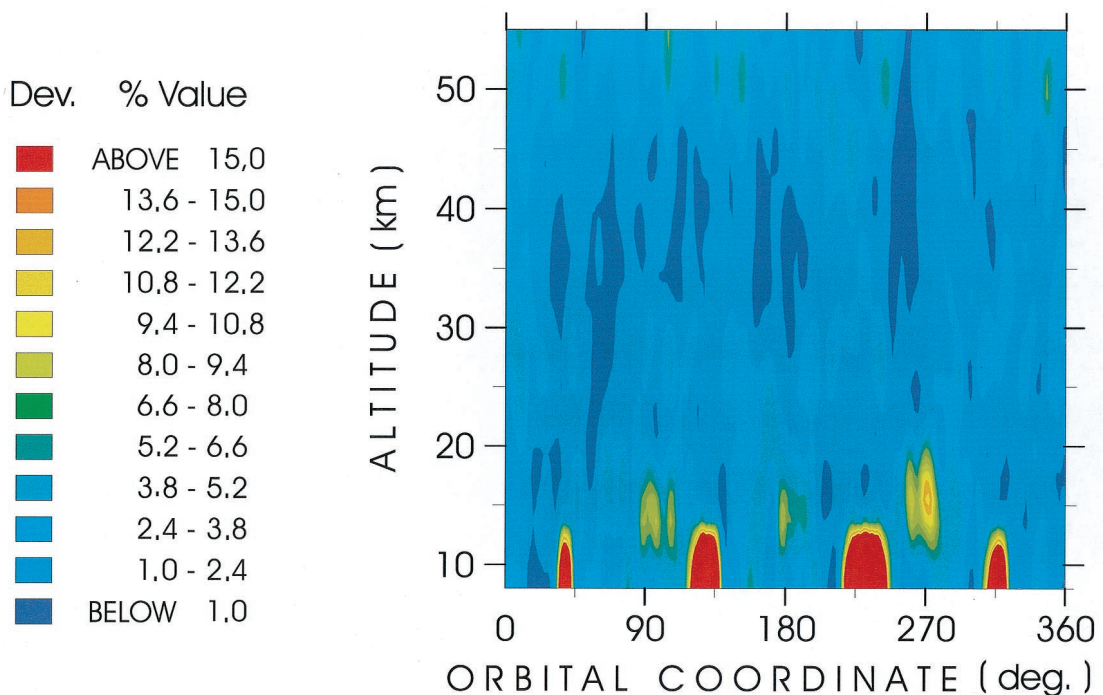


Fig. 4. Absolute values of the difference between VMR's retrieved by the geo-fit and reference VMR's.

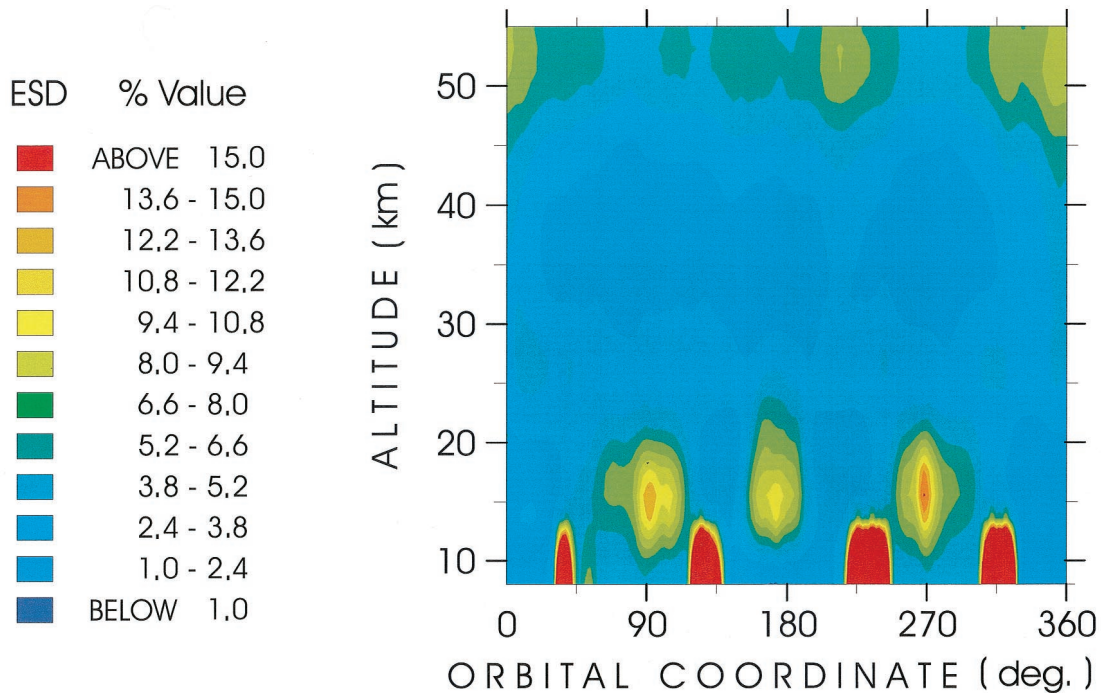


Fig. 5. Values of the ESD obtained by the geo-fit for a retrieval grid displaced to positions that are coincident with the ORM grids.

geo-fit and the ORM when they retrieve ozone VMR's in observational conditions similar to those used in the performance test discussed in the Section 4.

In principle it would be desirable to have the two systems analyze the same observations. However, it was soon clear that the performance of the ORM, even when it operates on the observations generated by a homogeneous atmosphere, was worse than that of the geo-fit. This fact is not surprising because, as we stated in Section 2, when one is determining the VMR at a location identified by a limb-scanning sequence the geo-fit gathers information not only from that sequence but also from observations of nearby sequences (see Fig. 1). As we needed results affected by comparable random errors, we had to increase the set of spectral points analyzed by the ORM by approximately a factor of 3. In this way the ORM provides better performance than does the corresponding geo-fit when they operate in a homogeneous atmosphere.

To compare the results of the two retrieval systems we had to adopt a retrieval grid that coincides with that of the ORM for the geo-fit. Therefore we associated to each sequence grid points lined up at the average value of the orbital coordinate of the target points of the sequence itself. All the profiles of the atmospheric model were interpolated to this average value to provide the input atmosphere to the ORM for the analysis of that sequence.

Figures 5 and 6 show ESD's and absolute deviations that resulted from the geo-fit in this comparison run. A comparison with Figs. 3 and 4 shows a worsening of the performance of the retrieval because the retrieval grid is no longer defined in the proximity of

the weighting-functions peak, as in the previous case. Figures 7 and 8 show ESD's and deviations that resulted from the retrievals made by the ORM over the 80 limb-scanning sequences of the whole orbit. The overall degradation of the performance because of the assumption of horizontal homogeneity can be clearly appreciated from a comparison of Figs. 7 and 8 with Figs. 5 and 6, respectively. A more-detailed estimate of this degradation can be obtained from a comparison of the results of individual limb-scanning sequences. Therefore we show two sequences that are representative of the overall behavior observed in the presence of low and high horizontal gradients. Figures 9 and 10 are related to a sequence close to 90° (equator) where, as can be seen from Fig. 2, a small horizontal variability occurs. Figure 9 shows the geo-fit percent errors as a function of altitude; in this figure dotted-dashed curves delimit the strip of ESD's and a solid curve joins the values of the deviations (marked by filled circles in the figure). Figure 10 shows the same quantities as in Fig. 9 but for the ORM analysis. Figures 11 and 12 are related to a sequence near the antarctic polar vortex (orbital coordinate, ≈160°) where high ozone gradients occur; they show, for the geo-fit and the ORM, respectively, the same quantities as in Figs. 9 and 10. An inspection of Figs. 5–12 shows that the performance of the ORM is slightly worse with respect to the geo-fit in the regions about the equator (where horizontal gradients are small) but dramatically deteriorates in the presence of strong horizontal gradients. Furthermore, for the ORM the observed deviations lie generally outside the strip that delimits the ESD values, and the discrepancies increase with horizontal gra-

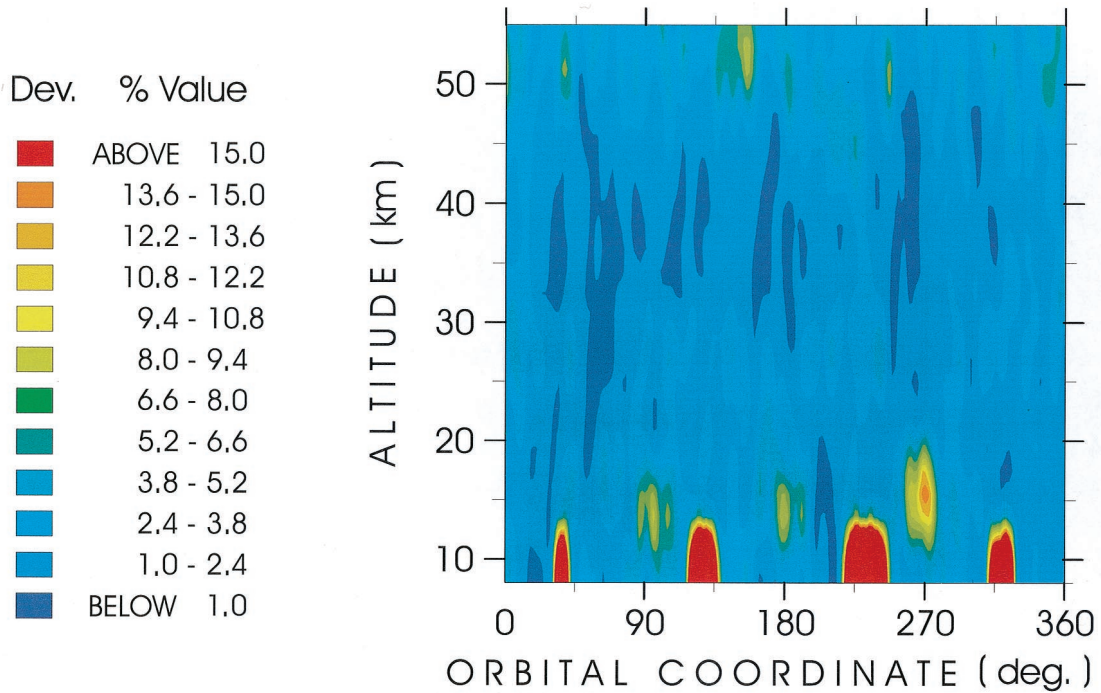


Fig. 6. Absolute values of the difference between VMR's retrieved by the geo-fit and reference VMR's for a retrieval grid displaced to positions coincident with the ORM grids.

dients. Because the ESD's are scaled by quantity  $q$  of Eq. (5), this behavior indicates that, even in the presence of horizontal gradients, the ORM makes a good fit of the observations (small ESD). Therefore the horizontal variability acts as a source of systematic error that does not show up in the residuals of the

fit. In other words, the degrees of freedom available to the ORM (that is, the parameters relative to the analyzed sequence) permit a good simulation of the observations, but one obtains the good fit by attributing incorrect values to the retrieved parameters.

The simulated observations used for the tests de-

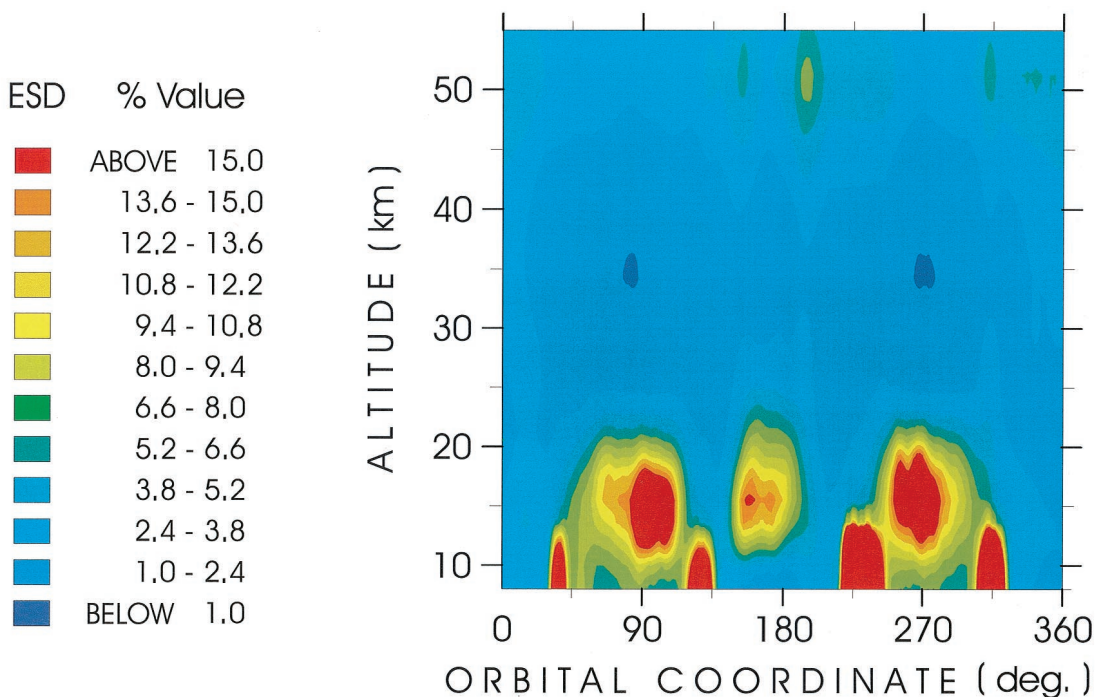


Fig. 7. Values of the ESD obtained by the ORM.

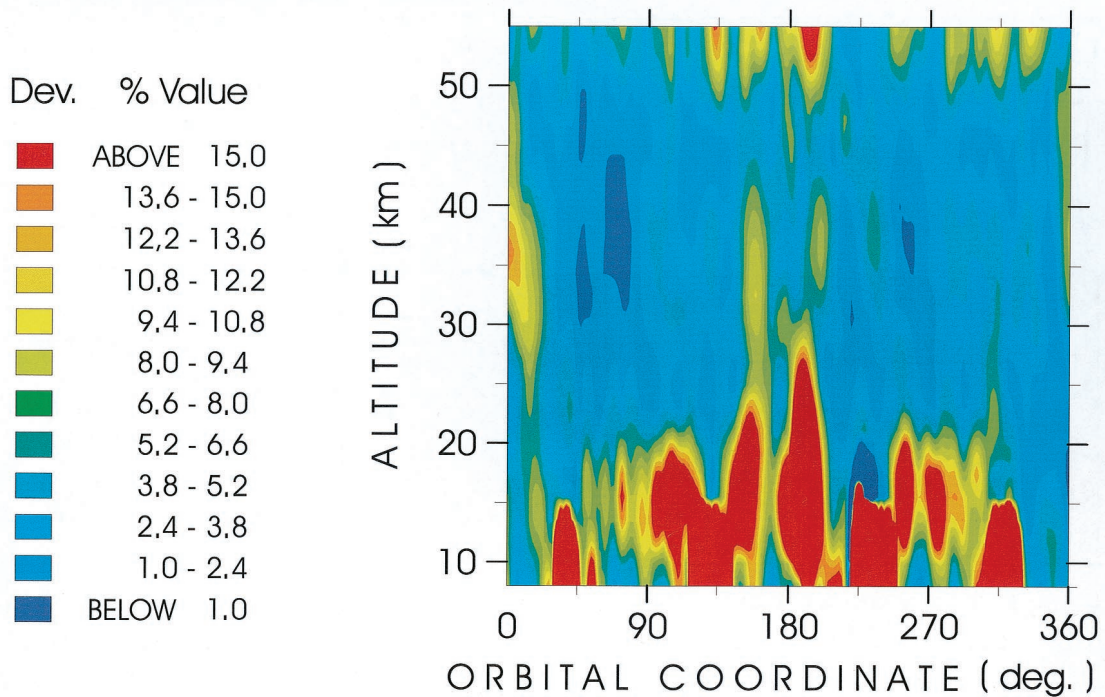


Fig. 8. Absolute values of the difference between VMR's retrieved by the ORM and reference VMR's.

scribed above were generated with an atmospheric model that is horizontally inhomogeneous not only with respect to ozone but also with respect to all other atmospheric constituents and, in particular, to pressure and temperature. Therefore we wonder which part of the errors for the ORM retrievals is generated by these other quantities. The effect of all the atmospheric constituents but ozone is negligible because, when the microwindow database was built,<sup>15</sup> the influence of interfering gases in the microwindows was minimized. To estimate the effect of pressure and temperature, we repeated the ORM retrievals on observations generated by use of an atmosphere that is horizontally homogeneous with respect to pressure and temperature. As an exam-

ple of the results of this test, we show in Fig. 13 the errors relative to the sequence about the antarctic polar vortex already considered in Fig. 12. From a comparison of Figs. 12 and 13 it is evident that a considerable part of the errors of the ORM is due to the assumption of horizontal homogeneity of pressure and temperature. The statistics for the deviations along the whole orbit indicate that this assumption accounts for ~50% of the degradation of the ORM retrievals.

## 6. Computational Strategy

In the performance test discussed in Subsection 4.D the computational problem was characterized by the following dimensions. The retrieval was simulated

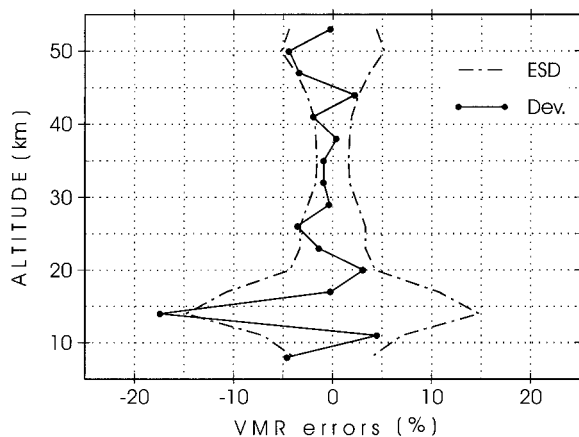


Fig. 9. Geofit errors for a sequence near the equator. Dotted-dashed curves delimit the strip of percent ESD's. The solid curve joins the values of the percent deviations (marked by filled circles).

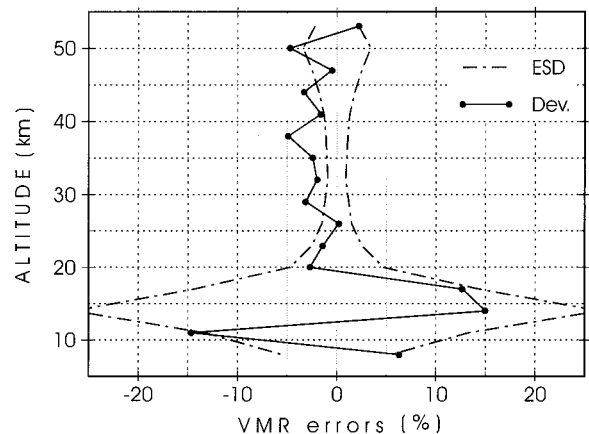


Fig. 10. ORM errors for the same limb-scanning sequence, with the same identifications of the curves, as in Fig. 9.

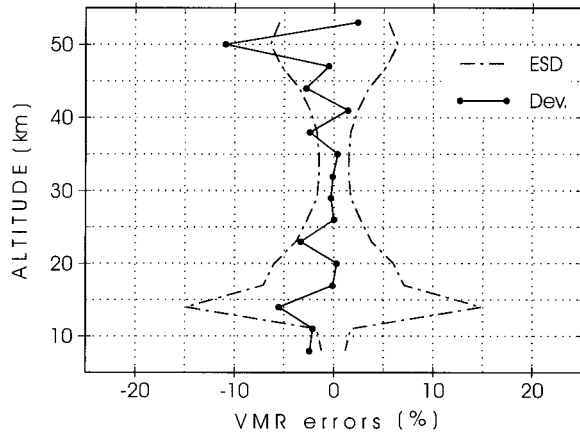


Fig. 11. Geofit errors as a function of altitude for a sequence crossing the antarctic polar vortex (orbital coordinate,  $\approx 160^\circ$ ). Curves have the same meanings as for Fig. 10.

by analysis of a set of microwindows that correspond to 949 spectral points for each of the 80 limb-scanning sequences. Therefore a total of 75,920 observations were analyzed. With a boundary imposed at 80 km the atmosphere was subdivided into 38 levels and 360 radii for a total of 13,320 cloves. The retrieval grid (defined by the nominal location of the tangent altitudes) corresponds to 1280 VMR parameters. For the atmospheric continuum, each microwindow identifies a parameter to be retrieved at each retrieval grid point. However, the number of atmospheric-continuum parameters is reduced because not all microwindows are used at the individual tangent altitudes of a limb-scanning sequence. Furthermore, the atmospheric continuum was required to be equal to zero above a threshold altitude of 30 km. The resultant number of atmospheric-continuum parameters was 2240 for a total of 3520 parameters that were determined in this test.

In Subsection 3.B we recalled that the core of the

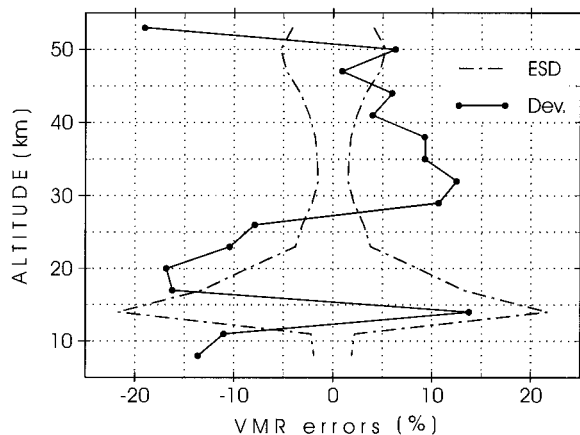


Fig. 12. ORM errors as a function of altitude for the same limb-scanning sequence as in Fig. 11. Curves have the same meaning as for Fig. 10.

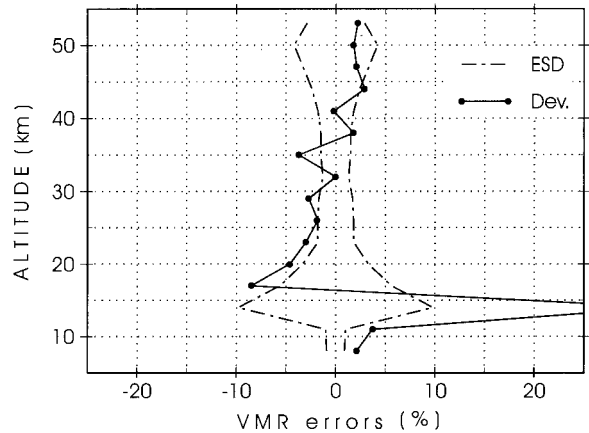


Fig. 13. ORM errors as a function of altitude for the same limb-scanning sequence as in Fig. 11 for observations generated by an atmosphere that is horizontally homogeneous with respect to pressure and temperature. Curves have the same meaning as in Fig. 10.

retrieval system resides in the calculation of Eq. (3). The dimension of the arrays in Eq. (3) are

$$\mathbf{y}(n), \quad \mathbf{K}(m, n), \quad \mathbf{S}_n(m, m), \quad \mathbf{n}(m),$$

where  $m$  is the number of analyzed spectral points and  $n$  is the number of parameters of the retrieval. In the performance test we had  $m = 75,920$  and  $n = 3520$ . Even if a real  $\times 4$  representation is used, the storage of the arrays in Eq. (3) would require more than 24 Gbytes of computer memory. If we also consider that intermediate results should be stored and the CPU time required by matrix algebra, the number of computations involved in Eq. (3) appears beyond the capability of most modern mainframes. To overcome this problem we adopted a strategy based on the physical meaning of the quantities in Eq. (3).

In matrix  $\mathbf{K}$ , each column refers to a retrieved parameter and each row refers to an observation and contains the derivatives of that observation with respect to all the retrieved parameters. It is easy to see that only minor sections of each row will contain entries that differ from zero; these are the sections that correspond to the parameters that lie in the area surrounding the geolocation of the observation. With a suitable layout of the parameters, matrix  $\mathbf{K}$  can be compressed such that only the sections of a row that contain values different from zero are computed and stored. Auxiliary vectors provide information about the position of the stored entries in matrix  $\mathbf{K}$ . A similar compression can be applied to matrix  $\mathbf{S}_n^{-1}$ , which has a block-diagonal structure (with the assumption that the observations of different microwindows are not correlated). The compression of these two matrices also permits multiplications involving zero elements to be avoided, hence reducing by orders of magnitude the number of operations needed for the matrix products of Eq. (3).

We computed entries of matrix  $\mathbf{A} = \mathbf{K}^T \mathbf{S}_n^{-1} \mathbf{K}$  without storing the product between the first two matrices. However, because  $\mathbf{K}^T$  is compressed along its

columns, it is necessary to store, in turn, a column of  $\mathbf{K}^T \mathbf{S}_n^{-1}$  to be replaced by the next column when its contribution has been used for all entries of  $\mathbf{A}$ . The matrix inversion is then performed with an efficient algorithm that exploits the symmetry of matrix  $\mathbf{A}$ . The result of the inversion gives matrix  $\mathbf{V}_y$  [see Eq. (6)], which overwrites  $\mathbf{A}$  and is stored because, at convergence of the iterative procedure, it represents the variance–covariance of the retrieved parameters.

From a mathematical point of view  $\mathbf{V}_y$  is a square-sparse matrix with dimension  $n$  that cannot be compressed. However, if we recall that its entries represent the covariance between two parameters, we can suppose that, in each row, moving away from the geolocation of the parameter identified by that row, the weighted contribution of the entries will decrease to a negligible value. With a few tests we established a threshold value that permits the sections of the row that contain nonnegligible entries to be identified. Therefore we scan the rows of  $\mathbf{V}_y$  to define auxiliary vectors used, in the next step, to avoid multiplications that involve negligible elements. This expedient permits reduction by approximately a factor of 7 of the CPU time required for computation of the remaining part of Eq. (3) that is in the computation of  $\mathbf{y} = \mathbf{V}_y \mathbf{K}^T \mathbf{S}_n^{-1} \mathbf{n}$ . In calculating this expression, one can compute the entries of vector  $\mathbf{y}$  by storing only an intermediate vector of dimension  $m$ . When the described strategy was adopted, the memory requirement for the computation of Eq. (3) was reduced to reasonable values.

Another demanding step from the point of view of computer time is the calculation of cross sections (see Subsection 3.A.6). This calculation must be fully performed when the forward model is used in the iterative procedure for the first time. However, while calculating Eq. (2) we store in a binary file the part of the summation that excludes the gas that is the target of the retrieval. In the subsequent use of the forward model, only the term relative to the target gas needs to be calculated; the remaining part is read from the file.

Apart from the optimizations described, no other effort was devoted to speeding up the computing program. Indeed, in writing this software we chose to emphasize clarity of a scientific code rather than computational efficiency.

The overall memory (RAM) requirement for running the performance test presented in Subsection 4.D is  $\sim 700$  Mbytes; whereas the disk space allotted for the storage of cross-sectional terms is  $\sim 3$  Gbytes. This test, run on CPU EV6 21264 of a DEC-AlphaServer DS20 computer requires 58 min of computing time distributed roughly as follows: 20% for calculation of cross sections, 30% for calculation of radiative transfer and derivatives, and 45% for the matrix algebra involved in the calculation of Eq. (3).

## 7. Conclusions

A new approach (termed geo-fit) has been proposed for analysis of limb-scanning observations that con-

tinually sound the atmosphere from an orbiting platform. In the case of a spectrometer that observes the atmosphere along the track of the orbit, this approach fully accounts for the atmospheric variability along the line of sight. As a consequence the retrieved atmospheric parameters are not affected by the error associated with the assumption of horizontal homogeneity. In a geo-fit, observations from a whole orbit are analyzed simultaneously, permitting full use to be made of the information that each observation brings from its line of sight.

The proposed retrieval method has been implemented with a computer program and tested on simulated observations of the MIPAS experiment. These tests show that the accuracy of each retrieved parameter is improved by the gathering of information by the geo-fit from all the observations affected by that parameter. Furthermore, the accuracy provided by the geo-fit is consistent with the uncertainty that is due to spectral noise and is not correlated with the horizontal variability of the atmosphere. This proves that the geo-fit eliminates systematic errors caused by atmospheric variability.

We employed the new retrieval method to estimate the errors made when horizontal homogeneity in the atmosphere is assumed. It was shown that the character of these errors is purely systematic in the sense that the errors tend not to show up in the residuals of the fitting procedure. The size of the errors is such as to compromise the validity of the retrieval when the horizontal variability of the atmosphere becomes important. Furthermore, it was shown that  $\sim 50\%$  of the error is due to the assumption of horizontal homogeneity with respect to temperature and pressure. The influence of pressure and temperature on the accuracy of the VMR retrievals suggests that one should determine these physical quantities also by taking into account their horizontal variability in the atmosphere.

The size of the problem of fitting data from a whole orbit is such that some computational artifice is needed to limit the demands on computer resources. We described a few expedients adopted to make handling the problem feasible. A test case of retrieval analysis was described that determines ozone distributions along a whole orbit. The computing time required for this analysis, on a medium-sized scalar machine, is less than 60% of the time required by the spacecraft to complete an orbit. Considering the growth in the performance of modern computers and the optimizations that are possible in an operational code, we can conclude that the geo-fit approach could be used for real-time retrieval of many atmospheric parameters.

The authors are grateful to M. Chipperfield for providing the SLIMCAT simulations used as the atmospheric model, L. Magnani for technical assistance in running the ORM retrievals, and B. Carli for his suggestions on the preparation of the manuscript.

## References

1. M. Ridolfi, B. Carli, M. Carlotti, T. von Clarmann, B. M. Dinelli, A. Dudhia, J. M. Flaud, M. Höpfner, P. E. Morris, P. Raspollini, G. Stiller, and R. J. Wells, "Optimized forward model and retrieval scheme for MIPAS near-real-time data processing," *Appl. Opt.* **39**, 1323–1340 (2000).
2. B. Carli, M. Ridolfi, P. Raspollini, B. M. Dinelli, A. Dudhia, and G. Echle, "Study of the retrieval of atmospheric trace gas profiles from infrared spectra," in *Final Report of ESA Study 12055-96-NL-CN* (European Space Research and Technology Centre, Noordwijk, The Netherlands, 1998).
3. G. P. Stiller, M. Höpfner, M. Kuntz, T. von Clarmann, G. Echle, H. Fischer, B. Funke, N. Glatthor, F. Hase, and S. Zorn, "The Karlsruhe optimized and precise radiative transfer algorithm (KOPRA): realization, model error assessment, and a *posteriori* justification," in *Proceedings of ESAMS'99, European Symposium on Atmospheric Measurements from Space* (European Space Research and Technology Center, Noordwijk, The Netherlands, 1999), pp. 749–756.
4. H. E. Fleming, "Satellite remote sensing by the technique of computed tomography," *J. Appl. Meteorol.* **21**, 1538–1549 (1982).
5. J. Zhang and Y. Xun, "Advanced retrieval method in satellite remote sensing atmosphere: the technique of computed tomography," in *Optical Remote Sensing of the Atmosphere and Clouds*, J. Wang, B. Wu, T. Ogawa, and Z. Guan, eds. *Proc. SPIE* **3501**, 207–214 (1998).
6. C. J. Marks and C. D. Rodgers, "A retrieval method for atmospheric composition from limb emission measurements," *J. Geophys. Res.* **98**, 14,939–14,953 (1993).
7. A. Friedle, M. Gobel, S. Hilgers, H. Kemnitzer, K. J. Ressel, G. Schwarz, S. Slijkhuis, T. Steck, T. von Clarmann, G. Echle, and M. Höpfner, "The MIPAS level 2 off-line processor: realization and test results," in *Proceedings of ESAMS'99, European Symposium on Atmospheric Measurements from Space*, (European Space Research and Technology Center, Noordwijk, The Netherlands, 1999), pp. 509–512.
8. A. Goldman, D. G. Murcray, F. J. Murcray, W. J. Williams, and J. N. Brooks, "Distribution of water vapor in the stratosphere as determined from balloon measurements of atmospheric emission spectra in the 24–29- $\mu\text{m}$  region," *Appl. Opt.* **12**, 1045–1053 (1973).
9. M. Carlotti, "Global fit approach to the analysis of limb-scanning atmospheric measurements," *Appl. Opt.* **27**, 3250–3254 (1988).
10. J. T. Houghton, *The Physics of Atmospheres*, 2nd ed. (Cambridge U. Press, Cambridge, 1986).
11. M. Carlotti, and B. Carli, "Approach to the design and data analysis of a limb-scanning experiment," *Appl. Opt.* **33**, 3237–3249 (1994).
12. European Space Agency, ed., "ENVISAT-MIPAS: an instrument for atmospheric chemistry and climate research," ESA Rep. SP-1229. (European Space Research and Technology Center, Noordwijk, The Netherlands, March 2000).
13. M. P. Chipperfield, "Multiannual simulations with a three-dimensional chemical transport model," *J. Geophys. Res.* **104**, 1781–1805 (1999).
14. S. A. Clough, F. X. Kneizys, and R. W. Davis, "Line shape and the water vapour continuum," *Atmos. Res.* **23**, 229–241 (1989).
15. T. von Clarmann and G. Echle, "Selection of optimized micro-windows for atmospheric spectroscopy," *Appl. Opt.* **37**, 7661–7669 (1998).